ARL-TR-9052 ● SEP 2020

DEVCOM ARMY RESEARCH LABORATORY

Optical Spectroscopy of Low-Phonon, Holmium-Doped Barium Fluoride (BaF_2) Single Crystals

by Ei Ei Brown, Zackery Fleischman, Jason McKay, and Mark Dubinskii

NOTICES

Disclaimers

The findings in this report are not to be construed as an official Department of the Army position unless so designated by other authorized documents.

Citation of manufacturer's or trade names does not constitute an official endorsement or approval of the use thereof.

Destroy this report when it is no longer needed. Do not return it to the originator.

ARL-TR-9052 ● SEP 2020

Optical Spectroscopy of Low-Phonon, Holmium-Doped Barium Fluoride (BaF_2) Single Crystals

Ei Ei Brown, Zackery Fleischman, and Mark Dubinskii
Sensors and Electron Devices Directorate, CCDC Army Research Laboratory

Jason McKay
General Technical Services, LLC

REPORT DOCUMENTATION PAGE

Form Approved
OMB No. 0704-0188

1. REPORT DATE *(DD-MM-YYYY)*	2. REPORT TYPE	3. DATES COVERED (From - To)
September 2020	Technical Report	January 1, 2019–December 31, 2019

4. TITLE AND SUBTITLE
Optical Spectroscopy of Low-Phonon, Holmium-doped Barium Fluoride (BaF_2) Single Crystals

5a. CONTRACT NUMBER

5b. GRANT NUMBER

5c. PROGRAM ELEMENT NUMBER

6. AUTHOR(S)
Ei Ei Brown, Zackery Fleischman, Jason McKay, and Mark Dubinskii

5d. PROJECT NUMBER

5e. TASK NUMBER

5f. WORK UNIT NUMBER

7. PERFORMING ORGANIZATION NAME(S) AND ADDRESS(ES)
CCDC Army Research Laboratory
ATTN: FCDD-RLS-RL
Adelphi, MD 20783-1138

8. PERFORMING ORGANIZATION REPORT NUMBER
ARL-TR-9052

9. SPONSORING/MONITORING AGENCY NAME(S) AND ADDRESS(ES)

10. SPONSOR/MONITOR'S ACRONYM(S)

11. SPONSOR/MONITOR'S REPORT NUMBER(S)

12. DISTRIBUTION/AVAILABILITY STATEMENT
Approved for public release; distribution is unlimited.

13. SUPPLEMENTARY NOTES
ORCID ID(s): Ei Ei Brown, 0000-0002-4102-1006

14. ABSTRACT

The development of new solid-state laser materials for mid-IR laser sources continues to be of significant interest for potential applications in remote sensing of biochemical agents, medicine, and IR spectroscopy. Fluorescent materials based on holmium (Ho^{3+})-doped crystals and glasses with narrow phonon spectra cover a wide wavelength range between approximately 1–4 μm. In this work, spectroscopic characterization of the IR emission properties of trivalent Ho^{3+}-doped barium fluoride (BaF_2) was explored. BaF_2 is particularly attractive due to its low maximum phonon energy of approximately 330 cm^{-1}, which leads to low nonradiative decay rates and efficient IR fluorescence. The studied Ho^{3+}-doped BaF_2 material was grown by the Bridgman technique. Using approximately 890-nm excitation, IR emissions centered at approximately 2.0, 2.85, and 3.90 μm were observed from Ho^{3+}:BaF_2 corresponding to the $5I7 \rightarrow 5I8$, $5I6 \rightarrow 5I7$, and $5I5 \rightarrow 5I6$ transitions of Ho^{3+} ions. Spectroscopic results and data modeling including Judd–Ofelt analysis, transitions cross sections, and fluorescence dynamics are discussed.

15. SUBJECT TERMS
rare-earth doped, mid-infrared, laser, holmium, IR, Ho^{3+}

16. SECURITY CLASSIFICATION OF:			17. LIMITATION OF ABSTRACT	18. NUMBER OF PAGES	19a. NAME OF RESPONSIBLE PERSON
a. REPORT	b. ABSTRACT	c. THIS PAGE			Ei Ei Brown
Unclassified	Unclassified	Unclassified	UU	24	19b. TELEPHONE NUMBER (Include area code) (301) 394-2293

Contents

List of Figures

List of Tables

1. Introduction

The mid-IR region has recently been a focus area for solid-state laser development because of its uniquely high 3- to 5-µm transmittance through air, as shown in Fig. 1.[1–6] The region overlaps with the energies of the vibrational modes of molecules, and has a variety of applications for environmental monitoring and chemical detection, as well as potential applications in remote sensing of biochemical agents, medicine, and IR spectroscopy. Some applications for mid-IR lasers include free-space communication and remote sensing of trace gases and vapors for pollution detection, as well as blood and breath analysis.

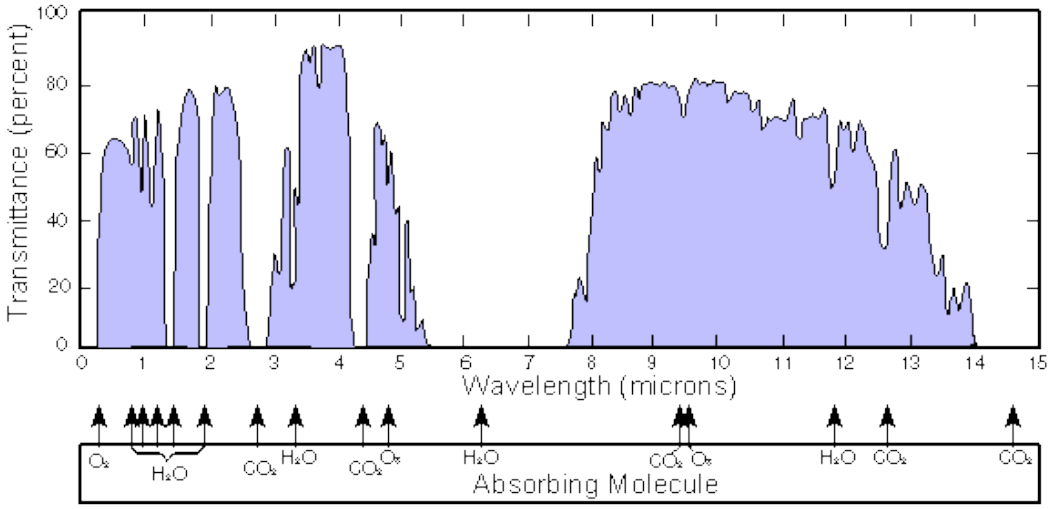

Fig. 1 Transmittance of the atmosphere

The development of rare-earth (RE)-doped host materials with low maximum phonon energies has attracted a great deal of interest for applications in solid-state lasers.[1–7] This is due to the reduced multiphonon relaxation rates that such host materials provide, which lead to higher laser emission efficiencies. Fluorites (calcium fluoride [CaF_2], strontium fluoride [SrF_2], and barium fluoride [BaF_2]) are laser hosts of interest due to their low phonon energies, high thermal conductivities, and compatibility with RE dopants.[8–12] The trivalent RE holmium (Ho^{3+}) ion is a favorable optically active center for applications in solid-state gain media. Laser oscillation and mid-IR emission properties from Ho^{3+}-doped crystals have been observed in the mid-IR wavelength region at approximately 3.9 µm due to the transition between the $^5I_5$ and $^5I_6$ state of Ho^{3+} ions.[1,13,14] More recently, the enhancement of 3.9-µm emission from Ho^{3+} through thulium (Tm^{3+}) sensitization has been reported in BaF_2 via approximately 800-nm excitation.[12]

In this work, we present results of spectroscopic investigations of mid-IR (3–5 μm) emission properties of Ho^{3+}:BaF_2 crystals. The Judd–Ofelt (J-O) theory was applied to estimate the radiative rates, radiative lifetimes, and branching ratios for the main IR transitions. The emission cross sections were determined for the several emission bands of interest for IR laser applications.

2. Experimental Details

2.1 Material Processing and Physical Properties

The studied Ho^{3+}-doped BaF_2 crystals were 5-cm-long cylindrical boules that were grown by the Bridgman technique. There were various Ho^{3+} concentrations in the BaF_2 samples, which were approximately 5.6 mm thick and 1 cm in diameter. Waxing and cutting of the investigated samples was performed prior to spectroscopic measurements. To cut the samples, mounting wax was melted on a glass slide and the boule was placed on the wax before it hardened. After the boule was firmly set on the glass slide, a cup of wax was melted to pour into a housing created by wrapping masking tape around the glass slide. The masking tape left approximately 1 cm of space around the boule, as illustrated in Fig. 2. Once the wax hardened, the tape was removed and, in an attempt to make the wax into a rectangular figure, the wax was melted on a hot plate on all sides until a rectangle was created.

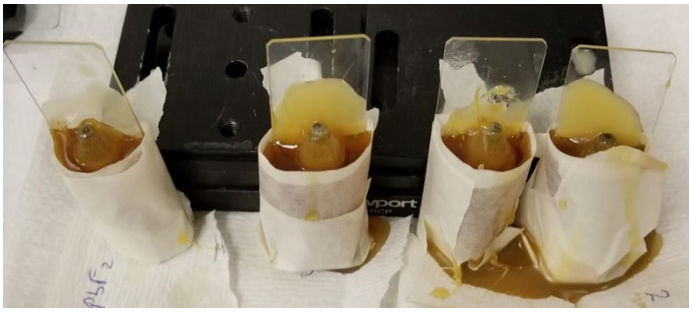

Fig. 2 Ho^{3+}:BaF_2 boules cooling in the wax casing for processing

Then, the sample was cut by a diamond saw (Fig. 3a) at a slow rate to ensure that the boule would not break or crack. After this process, the cut sample was polished by hand on silicon carbide polishing discs starting with 30-μm grit and working down to eventually using a 1-μm-grit disc. This ensures that the sample is fully transparent on the surface and there are no rough spots that could cause undesired scattering. Figure 3b shows the image of Ho^{3+}:BaF_2 crystals that were cut and polished.

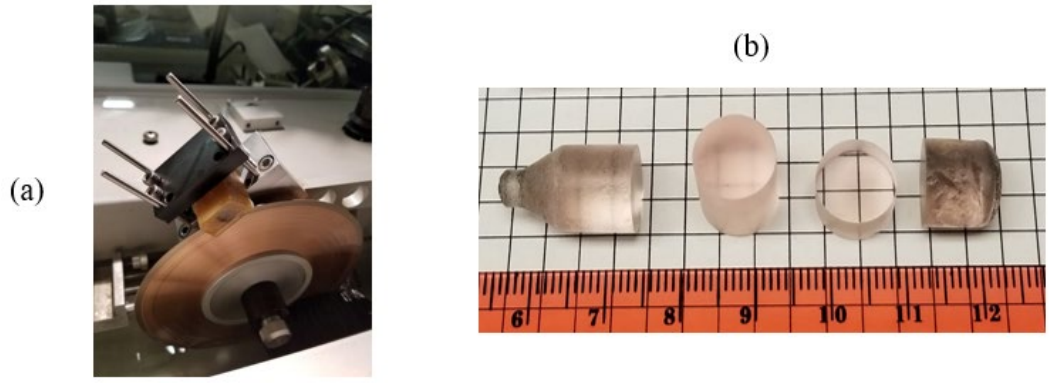

Fig. 3 a) Diamond saw cutting through the sample and b) Ho^{3+}:BaF_2 samples cut and polished

BaF_2 has a cubic crystal structure with a space group symmetry of Fm3m. The unit cell parameter is a = 0.62 nm and the number of molecules per unit cell is Z = 4.[11,12] BaF_2 has the density of 4.89 g/cm^3. It can be assumed that RE ions are incorporated into the divalent Ba^{2+} lattice sites, which require a charge compensation mechanism. It was reported that, for RE doped into fluorites,[11,12,15] the charge is compensated for by an interstitial fluorine ion at the nearest neighbor position of C_{3v} symmetry. Some of the physical properties of BaF_2 crystal are listed in Table 1.[11,12]

Table 1 Physical characteristics of BaF_2 crystal

Properties	BaF_2
Transparency	0.2–14 μm
Refractive index	1.475
Thermal conductivity	6 $Wm^{-1}K^{-1}$
Thermal expansion coefficient	18.1 10^{-6}/K
Maximum phonon energy	~330 cm^{-1}

2.2 Spectroscopic Measurements

Room-temperature absorption spectra were recorded using a Cary 6000i UV-visible (Vis)-near IR spectrophotometer and a Nicolet 6700 Fourier transform IR spectrometer. All mid-IR fluorescence spectra were excited by a continuous-wave Spectra-Physics Tsunami titanium (Ti):sapphire laser (800–905 nm). Either a Horiba Fluorolog-3 system with an iHR-320 monochromator (λ_{blaze}: 2 μm, 300 grooves/mm) or a Princeton Instruments Acton SpectraPro 0.15-m monochromator (λ_{blaze}: 4 μm, 150 grooves/mm) was used to collect the mid-IR emissions. The emission signal was recorded by an Infrared Associates liquid-nitrogen-cooled indium antimonide detector in conjunction with a Stanford Research Systems SR830 dual-phase lock-in amplifier. Fluorescence decay

measurements were carried out using the output of a pulsed (10-ns pulses, 10 Hz) neodymium (Nd): yttrium aluminum garnet (YAG) pumped optical parametric oscillator (OPO) system. The decay signal was recorded with a homemade LabVIEW program using National Instruments data acquisition system. For temperature-dependent emission studies down to 77 K, the sample was mounted on the cold finger of a two-stage, closed-cycle helium refrigerator.

3. Results and Discussion

3.1 Absorption Spectra and Judd–Ofelt Analysis

The room-temperature absorption spectrum of Ho^{3+}:BaF_2 in the 400- to 2200-nm region is shown in Fig. 4a. The absorption cross section was calculated using a Ho^{3+} concentration of approximately 1.49×10^{20} cm^{-3} for the Ho^{3+}:BaF_2 crystal, as measured by Galbraith Laboratory, Inc., using inductively coupled plasma optical emission spectroscopy (ICP-OES) (Fig. 4b). The characteristic absorption bands of Ho^{3+} ions were centered at approximately 1970, 1167, 899, 643, 538, 485, 470, 450, and 416 nm. The average absorption wavelengths were determined using the relation $\langle\lambda\rangle = \int\lambda\alpha(\lambda)d\lambda / \int\alpha(\lambda)d\lambda$, where $\alpha(\lambda)$ is the absorption coefficient as a function of wavelength.

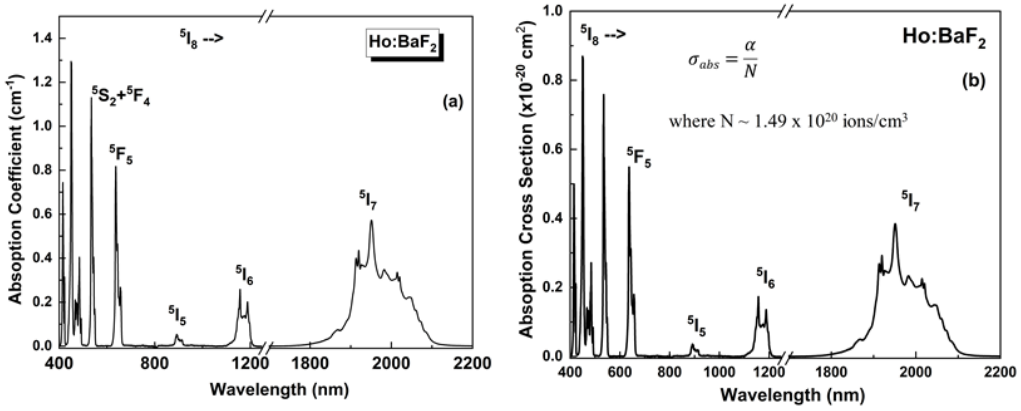

Fig. 4 a) Room-temperature absorption spectra of Ho^{3+}:BaF_2 in the 400- to 2200-nm spectral region. Intra-4f absorption bands from the $^5I_8$ ground state to higher excited states of Ho^{3+} are indicated. b) Absorption cross-section spectra of a Ho^{3+}:BaF_2 crystal.

The J-O theory allows the calculation of RE transition strengths and radiative rates of the levels from measured absorption spectra.[16,17] Nine absorption bands lying between 415 and 1970 nm were selected for evaluation of the three Ω_t parameters, known as the J-O intensity parameters. The intensities of the transitions can be distinguished by their line strength, *S*, for of each *SLJ* state. The experimentally

determined electric dipole transitions can be related to the integrated absorption coefficient by the following expression:

$$S_{meas}^{ed}(J \to J') = \frac{3hc(2J+1)}{8\pi^3 e^2 N_{RE} \lambda} \frac{9n}{(n^2+2)^2} \int \alpha(\lambda) d\lambda, \quad (1)$$

where J and J' are the total angular momentum of the initial and final states, respectively; h is Planck's constant; c is the speed of light; e is the electron charge; n is refractive index; N_{RE} is the concentration of Ho^{3+} ions in the crystal; λ is the mean wavelength of the absorption band; and $\int \alpha(\lambda)\, d\lambda$ is the integrated absorption coefficient.

The J-O intensity parameters Ω_t (t = 2,4,6) can be obtained by a least-squares fitting of the measured line strength to the calculated line strength of the corresponding transitions between J and J' manifolds in the following equations:

$$S_{calc}^{ed}(J \to J') = \sum_{t=2,4,6} \Omega_t \left| \left\langle (S,L)J \left\| U^{(t)} \right\| (S',L')J' \right\rangle \right|^2, \quad (2)$$

$$S_{calc}^{md}(J \to J') = \left(\frac{\hbar}{2mc} \right)^2 \left| \left\langle 4f^n[S,L]J \left\| L + 2S \right\| 4f^n[S',L']J' \right\rangle \right|^2 \quad (3)$$

where $\left\langle \left\| U^{(t)} \right\| \right\rangle$ are the doubly reduced matrix elements of the unit tensor.

The average transition wavelengths, integrated absorption coefficients, and experimental and calculated line strengths for Ho^{3+}:BaF_2 are presented in Table 2. The resulting values for the J-O parameters are Ω_2 = 0.293 × 10^{-20} cm^2, Ω_4 = 1.763 × 10^{-20} cm^2, and Ω_6 = 1.47 × 10^{-20} cm^2. The obtained J-O intensity parameters are within the range of values reported for other Ho^{3+}-doped fluoride materials (Table 3).[18–21]The root-mean-square (rms) deviation between measured and calculated electric dipole line strengths was determined using the following expression:

$$rms = \sqrt{\sum_{i=1}^{N} \frac{(S_{meas}^{ed} - S_{calc}^{ed})^2}{N-3}}, \quad (4)$$

where N is the number of absorption bands taken into account. The rms error was calculated to be approximately 0.19 × 10^{-20} cm^2, which is comparable to other rms values reported for Ho^{3+}-doped crystals.[18–21]

Table 2 Integrated absorption coefficients, measured, and calculated line strengths of Ho^{3+}:BaF_2

Transitions	Average wavelength	Transitions	Average wavelength	Transitions
$^5I_7$	1969.86	60.55	2.7	2.48
$^5I_6$	1167	9.467	0.737	1.087
$^5I_5$	898.78	1.245	0.126	0.154
$^5F_5$	642.86	11.318	1.599	1.59
$^5F_4$+$^5S_2$	537.63	10.345	1.748	1.798
$^5F_3$	484.65	2.786	0.522	0.508
$^3K_8$	470.22	2.239	0.433	0.297
$^5F_1$+$^5G_6$	449.86	10.57	2.135	2.138
$^5G_5$	416.56	4.47	0.976	0.779

Table 3 J-O intensity parameters for Ho^{3+}-doped fluoride crystals

Host	Ω_2 (10^{-20} cm^2)	Ω_4 (10^{-20} cm^2)	Ω_6 (10^{-20} cm^2)	δ (10^{-20} cm^2)	Reference no.
Ho:BaF_2	0.298	1.784	1.491	0.19	**This study**
Ho:CaF_2	0.018	0.57	0.587	…	18
Ho:LaF_3	1.03	0.98	0.31	…	19
Ho:$YLiF_4$	0.96	2.05	1.43	0.18	20
Ho:$LuLiF_4$	1.238	2.214	2.111	0.108	21
Ho:$GdLiF_4$	1.289	2.309	2.211	0.117	21

Note: La = lanthanum, Y = yttrium, Lu = lutetium, Gd = gadolinium.

Using the obtained emission line strengths, the radiative transition probabilities $A(J \rightarrow J')$ can be determined by the following equations:

$$A(J \rightarrow J') = \frac{64\pi^4 e^2}{3h(2J+1)}\left[\frac{n(n^2+2)^2}{9\lambda^3} S_{calc}^{ed}(J \rightarrow J') + n^3 S_{calc}^{md}(J \rightarrow J')\right], \quad (5)$$

$$A_t(J) = \sum_{J'} A(J \rightarrow J') \quad (6)$$

where A_t (J) is the total transition rate for a given J-manifold.

The radiative lifetime, τ_{rad}, is related to the radiative decay rate through

$$\tau_{rad} = \frac{1}{A_t(J)}. \quad (7)$$

Accordingly, the branching ratio, β, for the transition from an emitting level to a lower level is given by

$$\beta(J') = \frac{A(J \rightarrow J')}{A_t(J)}. \quad (8)$$

The radiative transition rates, branching ratios, and radiative and measured lifetimes are presented in Table 4. The emission cross sections were calculated using Füchtbauer–Ladenburg (F-L) equation[22]:

$$\sigma_{emiss}(\lambda) = \frac{\beta\lambda^5 I(\lambda)}{8\pi n^2 c\tau_{rad}\int \lambda I(\lambda)d\lambda} \quad (9)$$

where β and τ_{rad} are the branching ratio and radiative lifetime, respectively. $I(\lambda)$ is the emission intensity at wavelength λ and n is the refractive index of the host (n = 1.47).

Table 4 Calculated radiative transition probabilities (A_{ij}), branching ratios (β_{ij}), radiative (τ_{meas}), and measured (τ_{meas}) lifetimes of Ho^{3+}:BaF_2

Transitions	(nm)	A_{ij} (s^{-1})	β_{ij}	τ_{rad} (ms)	τ_{meas} (ms)
$^5I_7 \rightarrow {}^5I_8$	2010	48.06	1	20.8	17.0
$^5I_6 \rightarrow {}^5I_7$	2850	11.17	0.098	…	…
$^5I_6 \rightarrow {}^5I_8$	1190	103.4	0.902	8.73	6.8
$^5I_5 \rightarrow {}^5I_6$	3900	3.69	0.037	…	…
$^5I_5 \rightarrow {}^5I_7$	1650	56.81	0.571	…	…
$^5I_5 \rightarrow {}^5I_8$	910	38.93	0.392	10.05	0.026

3.2 Infrared Emission Studies

3.2.1 2 μm Emission

The Ho^{3+}:BaF_2 crystal exhibited broad emission band centered at approximately 2 μm ($^5I_7 \rightarrow {}^5I_8$) with a bandwidth of approximately 0.14 μm at full width at half maximum (Fig. 5). Following optical pumping at 0.89 μm, the room-temperature emission decay transient was nearly exponential with a lifetime value of approximately 17 ms. Using the J-O analysis, the radiative lifetime of the $^5I_7$ level was calculated to be approximately 20.8 ms, which is in good agreement with the calculated radiative lifetime (19.94 ms) obtained by Einstein's relationship,[23]

$$\tau_{calc} = \frac{\lambda^2}{8\pi c n^2}\left[\frac{g_1}{g_2}\int \sigma_{abs} d\bar{\nu}\right]^{-1} \quad (10)$$

where σ_{abs} is the absorption cross section (Fig. 5), λ is the average absorption wavelengths, c is the speed of light, n is the index of refraction, and g_1 and g_2 are the ground and excited state degeneracies, respectively.

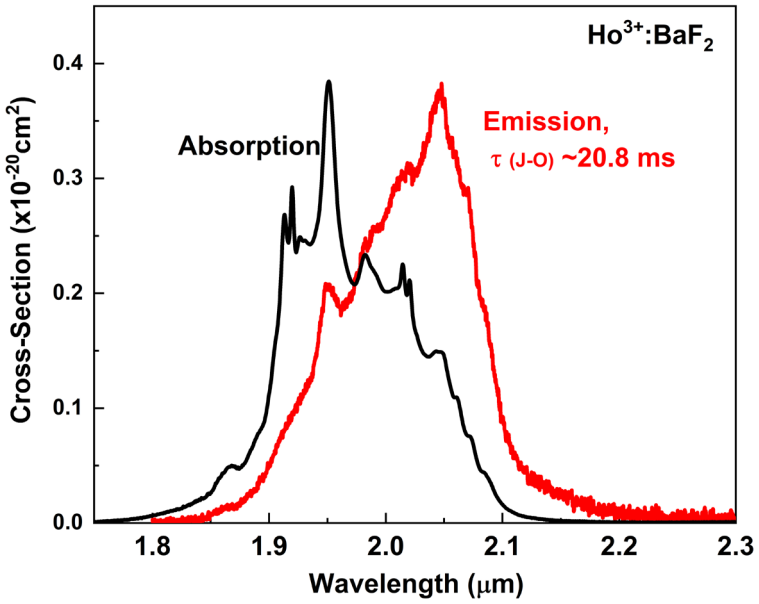

Fig. 5 Absorption and emission cross-section spectra of $^5I_7 \rightarrow {}^5I_8$ transition for Ho^{3+}:BaF_2

The small difference in the experimental (measured) lifetime and calculated radiative lifetime of the $^5I_7$ could be due to radiation trapping in the investigated Ho^{3+}:BaF_2 sample. Using the available spectroscopic data and radiative lifetime derived from a J-O analysis, the emission cross section of the $^5I_7 \rightarrow {}^5I_8$ emission transition was calculated for Ho^{3+}:BaF_2 using the F-L method (Eq. 9).[22] The peak emission cross section was determined to be approximately 0.38×10^{-20} cm^2, which is slightly smaller than Ho^{3+}:$YLiF_4$ (Ho^{3+}:YLF)[24] and Ho^{3+}:BaY_2F_8 (Ho^{3+}:BYF)[1] (Table 5); however, it was comparable to the reported value of approximately 0.39×10^{-20} cm^2 for Ho^{3+}:LaF_3.[19] Due to the quasi three-level nature of a potential approximately 2-μm laser based on the $^5I_7 \rightarrow {}^5I_8$ Ho^{3+} transition, a net gain cross section g (λ) can be calculated considering possible ground-state absorption losses at the laser wavelength[25]:

$$g(\lambda) = \beta\sigma_{emis}(\lambda) - (1-\beta)\sigma_{abs}(\lambda) \qquad (11)$$

where $\beta = N_{exc}/N_{tot}$ is the ratio of the number of excited Ho^{3+} ions relative to the total Ho^{3+} ion population, and σ_{emis} and σ_{abs} are the emission and absorption cross sections, respectively. The obtained gain cross-section spectra for β = 0, 0.25, 0.5, 0.75, and 1 are illustrated in Fig. 6. It can be noticed that nearly 25% population inversion is needed for Ho^{3+}:BaF_2 to achieve a positive gain at the longer wavelengths above 2.06 μm.

Table 5 Comparison of Ho^{3+}:BaF_2 and other Ho^{3+}-doped fluorides for emission cross sections, and radiative and measured lifetimes

Crystal	λ_{em}(μm)	$\sigma_{em}(\lambda)$ (10^{-20} cm^2)	τ_{rad} (ms)	τ_{meas} (ms)	σ-τ (10^{-20} cm^2.ms)
Ho:BaF_2	2.04	0.38	20.8	16.7	…
Ho:YLF (Walsh et al.[24])	2.06	0.75	13.9	14.0	…
Ho:BYF (Eichhorn[1])	2.06	1.18	…	17.9	…
Ho:LaF_3 (Hong et al.[19])	1.93	0.39	25.16	25.81	…
Ho:BaF_2	2.84	0.57	8.73	6.8	~3.9
Ho:BYF (Eichhorn[1])	2.85	0.28	…	5.45	~1.5
Ho:LaF_3 (Hong et al.[19])	2.85	0.63	18.99	10.37	~6.5
Ho:BaF_2	3.89	0.76	10.05	0.028	~0.02
Ho:BYF (Eichhorn[1])	3.89	~1.5		0.052	~0.08

Note: YLF = yttrium lithium fluoride, BYF = barium yttrium fluoride, LaF_3 = lanthanum trifluoride

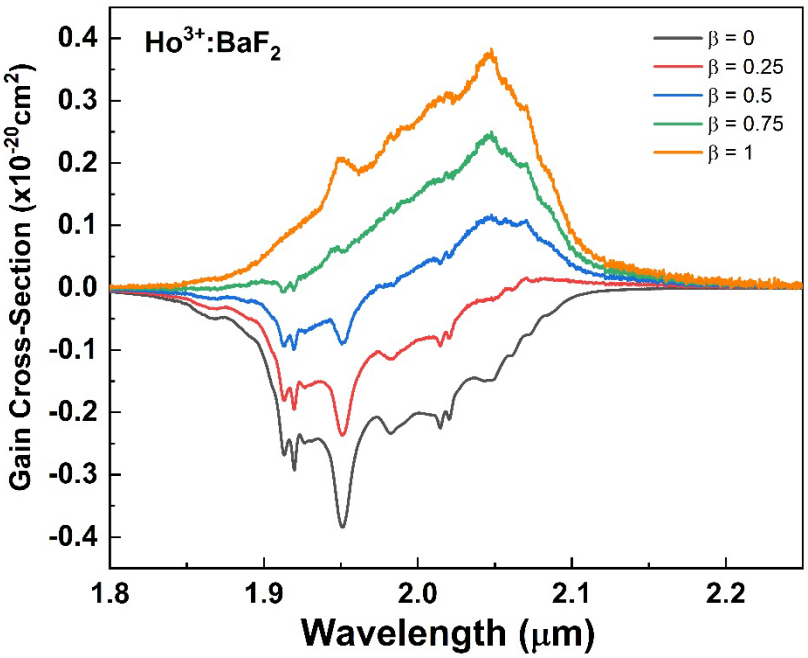

Fig. 6 Gain cross-section spectra of the 2-μm transition in Ho^{3+}:BaF_2 for different population inversion ratios (β = 0, 0.25, 0.5, 0.75, and 1)

3.2.2 2.8- and 3.9-μm Emissions

Figure 7 shows the room-temperature mid-IR emission spectra of the Ho^{3+}:BaF_2 crystal upon excitation at 0.89 μm using a Ti:sapphire laser. The spectra exhibited two emission bands centered at approximately 2.85 and 3.9 μm, which are attributed to the Ho^{3+} $^5I_6 \rightarrow {}^5I_7$ and $^5I_5 \rightarrow {}^5I_6$, respectively. A schematic diagram of the relevant lower Ho^{3+} levels indicating the excited transition and observed emission lines is shown in Fig. 7. The emission spectra were calibrated for the

experimental setup. It could be seen that both the approximately 2.85- and 3.9-μm emission bands were relatively broad ranging from 2.75 to 3.05 μm and 3.8 to 4.0 μm, respectively.

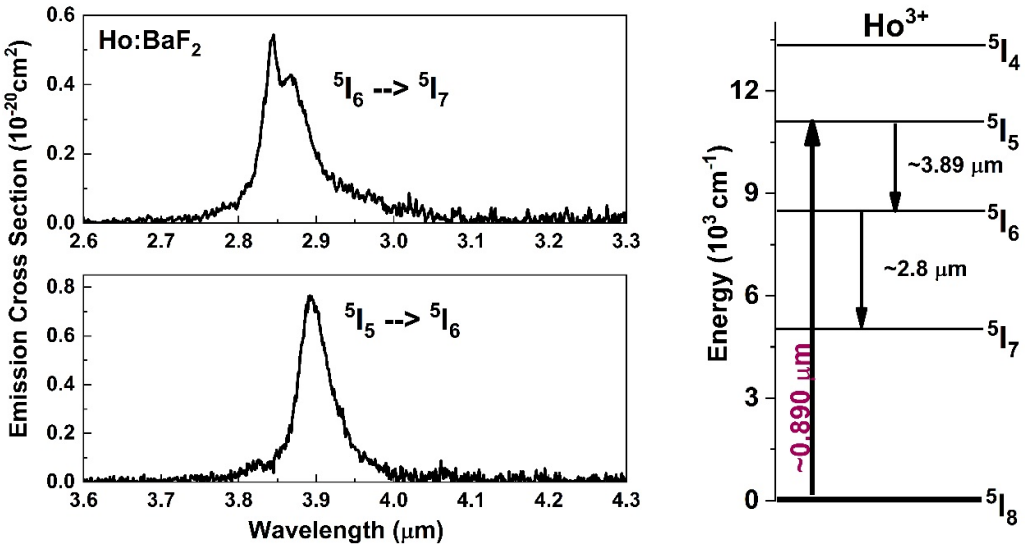

Fig. 7 Emission cross-section spectra of $^5I_6 \rightarrow {}^5I_7$ and $^5I_5 \rightarrow {}^5I_6$ transitions for the Ho^{3+}:BaF_2 crystal. The partial energy-level diagram of Ho^{3+} indicating the excitation level and the corresponding emission transitions is also shown on the right.

The decay transients of the $^5I_5$ and $^5I_6$ level were determined by using 891-nm excitation of pulsed Nd:YAG-pumped OPO system and can be seen in Fig. 8. The lifetime of the $^5I_6$ level was determined to be approximately 6.8 ms, which agrees reasonably well with the radiative lifetime of 8.73 ms determined by J-O analysis (see Table 4). The emission lifetime of the $^5I_5$ energy level exhibited a significantly shorter lifetime of approximately 26 μs. The observed $^5I_5$ level lifetime was similar to the reported value of 17.5 μs for 1% Ho^{3+}:BaF_2 and 28 μs for low concentration 0.35% Ho^{3+}:BaF_2.[12] J-O analysis yielded a radiative lifetime of 10.05 ms for the $^5I_5$ state, which suggests a quantum efficiency of less than 1% at room temperature. Such a low efficiency could be attributed to nonradiative decay processes such as multiphonon relaxations, energy transfer between RE ions, or energy transfer to other impurities in the crystal. The temperature dependence of the $^5I_5$ level decay time measurements are in progress in order to determine the multiphonon relaxation rate, which could be the most likely process for the reduced radiative emission efficiency. The shorter lifetime of the $^5I_5$ energy level makes it difficult for population inversion to occur unless high amounts of energy are pumped into the crystal or a higher Ho^{3+} concentration is achieved to increase absorption at the pump wavelength. However, pulsed laser operation at 3.9 μm has been demonstrated with Ho^{3+}:BaY_2F_8, which has a maximum phonon energy less than 500 cm^{-1}.[13]

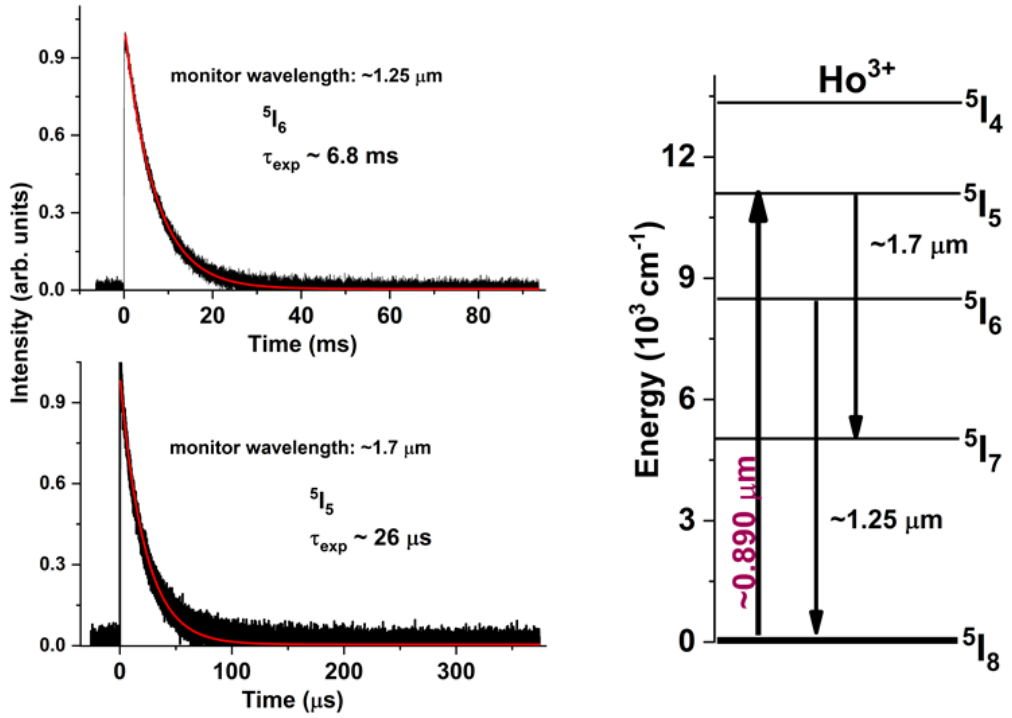

Fig. 8 Decay transients of Ho^{3+}:BaF_2 monitored at approximately 1.7 μm ($^5I_5$ → $^5I_7$) and 1.25 μm ($^5I_6$ → $^5I_8$) for room temperature. The partial energy-level diagram of Ho^{3+} indicating the pump level and the measured emission transitions is also depicted on the right.

The mid-IR emission cross-section spectra for Ho^{3+}:BaF_2 is expressed in Fig. 7 and the peak emission cross sections at 2.84 and 3.9 μm were determined to be 0.57×10^{-20} and 0.76×10^{-20} cm^2, respectively. The sigma-tau (σ-τ) product is an important parameter to characterize laser materials since its value is inversely proportional to the laser threshold under continuous wave excitation.[26] The resulting σ-τ product for 2.8- and 3.9-μm transition were calculated to be approximately 3.9×10^{-20} and 0.02×10^{-20} cm^2.ms, respectively. These emission cross sections and σ-τ product are comparable to other Holmium doped fluorides, as shown in Table 5.

The Ho^{3+}-doped BYF crystal shown in the table has demonstrated pulsed laser operation at 3.9 μm[13] using high Ho^{3+} concentration (30% Ho^{3+}:BYF). Comparing the samples, it could be possible to use a sample of Ho^{3+}:BaF_2 as a possible lasing material especially because the sample studied in this experiment was merely 3% Ho^{3+}.

The 3.9-μm emission arising from the $^5I_5$ to $^5I_6$ Ho^{3+} transition is a potential four-level laser system. As mentioned earlier, the most important requirement for laser emission is population inversion, which can only be maintained for a possible 3.9-μm laser if the $^5I_5$ level has a longer lifetime than the $^5I_6$ level. Figure 8 proved

that is not the case, since the $^5I_6$ level has a lifetime of 6.8 ms. This makes the continued population inversion rather difficult, as it results in bottlenecking or self-termination. This problem might be overcome through co-doping with a proper sensitizer ion (e.g., Nd^{3+}), which could provide an efficient excitation passage using its 808-nm absorption band. A schematic diagram of energy levels for Ho^{3+} and Nd^{3+} indicating the energy transfer process is illustrated in Fig. 9.[27] Overall, the observed spectroscopic parameters for Ho^{3+}:BaF_2 suggested that it could be a possible lasing candidate for mid-IR laser applications.

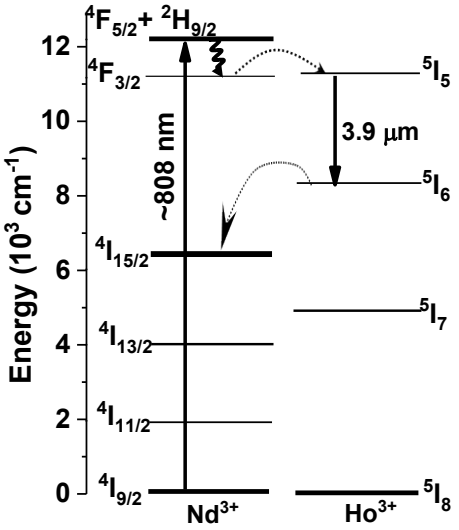

Fig. 9 A schematic diagram of energy levels for Ho^{3+} and Nd^{3+} indicating the energy transfer process

4. Conclusions

Preliminary results of the material preparation and IR spectroscopic properties of Ho^{3+}-doped BaF_2 crystals, grown by the Bridgman technique, were presented. The absorption spectrum of Ho^{3+}:BaF_2 displayed the characteristic Ho^{3+} transitions in the visible and IR spectral region. The J-O theory was applied and the J-O intensity parameters, radiative probabilities, branching ratios as well as radiative lifetimes were determined. Optical pumping into the $^5I_8$ → $^5I_5$ absorption band at approximately 800 nm resulted in the observation of several mid-IR Ho^{3+} fluorescence bands, which corresponds to the $^5I_7$ → $^5I_8$ (~2 μm), $^5I_6$ → $^5I_7$ (~2.8 μm), and $^5I_5$ → $^5I_6$ (~3.89 μm) transitions. The room-temperature fluorescence lifetimes of the first three excited states of Ho^{3+}:BaF_2 were determined to be approximately 17 ms ($^5I_7$), 6.8 ms ($^5I_6$), and 0.026 ms ($^5I_5$).

Using the J-O modeling and F-L method, the IR peak emission cross sections of approximately 2, 2.8, and 3.9 μm were determined to be 0.38 × 10^{-20},

0.57×10^{-20}, and 0.76×10^{-20} cm^2, respectively. The comparison of the absorption and emission cross sections for the $^5I_7 \rightarrow {}^5I_8$ transition indicates the possibility for a broadly tunable laser covering a region from approximately 2.0 μm to approximately 2.2 μm. The 2-μm gain cross-section spectra revealed that nearly 25% population inversion is required for Ho^{3+}:BaF_2 to achieve a positive gain at the long wavelength region between approximately 2.06 and 2.1 μm.

The emission cross section and long lifetime of 2.8 μm give Ho^{3+}:BaF_2 a large σ-τ product (~3.9×10^{-20} cm^2.ms), which is almost three times higher than the values reported for the known laser material Ho^{3+}:BYF crystal.[1] The obtained spectroscopic parameters for 2.8-μm emission compare favorably with other Ho^{3+}-doped fluorides, which underlines the potential of this material for 3-μm laser applications.

The 3.9-μm emission ($^5I_5 \rightarrow {}^5I_6$ transition) revealed a reasonably high emission cross section; however, with a short lifetime of approximately 0.026 ms. The longer lifetime of the lower excited state $^5I_6$, restricts the capability to effectively invert the population, therefore limiting the mode of operation of a potential Ho^{3+}:BaF_2 laser. It is found that the near-IR absorption at approximately 0.89 μm is extremely weak in this crystal with an absorption cross section of approximately 0.036×10^{-20} cm^2. These issues might be overcome through co-doping with a suitable sensitizer ion, for instance, Nd^{3+} or Tm^{3+} ions, which could provide an effective excitation channel using their approximately 800-nm absorption bands as well as efficient depopulation of the $^5I_6$ level for possible population inversion.[12,27]

5. References

1. Eichhorn M. Quasi-three-level solid-state lasers in the near and mid infrared based on trivalent rare earth ions. Appl Phys B. 2008;93:269–316.

2. Velazquez M, Ferrier A, Doualan J-L, Moncorge R. Rare-earth doped low phonon energy halide crystals for mid-infrared sources. In: Al-Khursan A, editor. Solid-State Laser. InTech, 2012, p. 119–142.

3. Tittel FK, Richter D, Fried A. Mid-infrared laser applications in spectroscopy, solid-state mid-infrared laser sources. Topics Appl Phys. 2003;89:445–510.

4. Kalisky Y. New trends in lasers and laser crystals. Optical Materials 13. 1999;135–139.

5. Seddon AB, Tang Z, Furniss D, Sujecki S, Benson TM. Progress in rare-earth doped mid-infrared fiber lasers. Opt Exp. 2010;18:26704–26719.

6. Isaenko L. Yelisseyev A, Tkachuk A, Ivanova S. New monocrystals with low phonon energy for mid-IR lasers. In: Ebrahim-Zadeh M, Sorokinda IT editors. Mid-infrared coherent sources and applications. Springer; 2008. p. 3–65.

7. Kaminskii AA. Crystalline lasers: physical processes and operating schemes. New York (NY): CRC Press; 1996.

8. Labbe C, Doualan JL, Camy P. Moncorge R. Thuau M. The 2.8 μm laser properties of Er^{3+} doped CaF_2 crystals. Opt Comm. 2002;209:193–199.

9. Svejkar R, Sulc J, Jelinkova H, Kubecek V, Ma W, Jiang D, Wu Q, Su L. Diode-pumped Er:SrF_2 laser tunable at 2.7 μm. Opt Mater Exp. 2018;8:1025–1030.

10. Orlovskii YV, Basiev TT, Pukhov KK, Glushkov NA, Alimov OK. Multiphonon relaxation of mid-IR transitions of RE ions in fluorite type crystals. In OSA Trends in Optics and Photonics (ASSP). Optical Society of America; 2004, paper 440.

11. Bitam A, Khiari S, Diaf M, Boubekri H, Boulma E, Bensalem C, Guerbous L, Jouart JP. Spectroscopic investigation of Er^{3+} doped BaF_2 single crystal. Opt Mater. 2018;82:104–109.

12. Orlovskii YV, Basiev TT, Pukhov KK, Alimov OK, Glushkov NA, Konyushkin VA. Low-phonon BaF_2:Ho^{3+}, Tm^{3+} doped crystals for 3.5-4 μm lasing. Opt Mater. 2010;32**:**599–611.

13. Stutz R, Miller HC, Dinndorf KM, Cassanho A, Jenssen HP. High-pulse-energy 3.9-μm lasers in Ho:BYF. Proc SPIE 5332, Solid State Lasers XIII: Technology and Devices; 2004 Jul 8.

14. Oyebola O, Hommerich U, Brown E, Trivedi SB, Bluiett AG, Zavada JM. Growth and optical spectroscopy of Ho-doped KPb_2Cl_5 for infrared solid-state lasers. J Cryst Grow. 2010;312:1154–1156.

15. Miller M, Wright JC. Single site multiphonon and energy transfer relaxation phenomena in $BaF_2:Er^{3+}$. J Chem Phys. 1978;68:1548.

16. Judd BR. Optical absorption intensities of rare-earth ion. Phys Rev. 1962;127:750–761.

17. Ofelt GS. Intensities of crystal spectra of rare-earth ions. J Chem Phys. 1962;37:511–520.

18. Bullock SR, Reddy BR, Venkateswarlu P, Nash-Stevenson SK. Site-selective energy upconversion in $CaF_2:Ho^{3+}$. J Opt Soc Am B. 1997;14:553–559 ().

19. Hong J, Zhang L, Zhang P, Xu M, Hang Y. Ho:LaF_3 single crystal as potential material for 2 μm and 2.9 μm lasers. Infr Phys Tech. 2016;76:636–640 ().

20. Li C, Guyot Y, Linares C, Moncorge R, Joubert MF. Radiative transition probabilities of trivalent rare-earth ions $LiYF_4$. OSA Proc. ASSL. In: Pinto AA, Fan TY, editors. 1993. vol. 15. p. 91–95.

21. Walsh B, Grew GW, Barnes N. Energy levels and intensity parameters of Ho^{3+} ions in $GdLiF_4$, $YLiF_4$ and $LuLiF_4$. J Phys Condens Matter. 2005;14:7643–7665.

22. Aull BF, Jenssen HP. Vibronic interactions in Nd:YAG resulting in nonreciprocity of absorption and stimulated emission cross sections. IEEE Quantum Electron. 1982;18:925–930.

23. Deloach LD, Page RH, Wilke GD, Payne SA, Krupke WF. Transition metal-doped zinc chalcogenides: spectroscopy and laser demonstration of a new class of gain media. IEEE J Quantum Electron. 1996;32:885–895.

24. Walsh B, Barnes NP, Bartolo BD. Branching ratios, cross sections, and radiative lifetimes of rare earth ions in solids: applications to Tm^{3+} and Ho^{3+} ions in $LiYF_4$. J Appl Phys. 1998;83:2772–2787.

25. Schweizer T, Jensen IT, Heumann E, Huber G. Spectroscopic properties and diode pumped 1.6 μm laser performance in Yb-codoped Er:$Y_3Al_5O_{12}$ and Er:Y_2SiO_5. Opt Comm. 1995;118:557–561.

26. Koechner W. Solid-state laser engineering. Springer Verlag; 1999.

27. Zhang P, Hang Y, Li Z, Chen Z, Yin H, Zhu S, Fu S, Li S, Xu M. Sensitization and deactivation effects of Nd^{3+} on the Ho^{3+}: 3.9 μm emission in a PbF_2 crystal. Opt Lett. 2017;42:2559–2562.

List of Symbols, Abbreviations, and Acronyms

Ba	barium
BaF_2	barium fluoride
BYF	barium yttrium fluoride
CaF_2	calcium fluoride
F	fluorine
Gd	gadolinium
Ho	holmium
ICP-OES	inductively coupled plasma optical emission spectroscopy
InSb	indium antimonide
IR	infrared
J-O	Judd–Ofelt
La	lanthanum
LaF_3	lanthanum trifluoride
Lu	lutetium
Nd	neodymium
NIR	near IR
OPO	optical parametric oscillator
RE	rare earth
SrF_2	strontium fluoride
Ti	titanium
Tm	thulium
UV	ultraviolet
Vis	visible
Y	yttrium
YAG	yttrium aluminum garnet
YLF	yttrium lithium fluoride

1 (PDF) DEFENSE TECHNICAL INFORMATION CTR DTIC OCA

1 (PDF) CCDC ARL FCDD RLD DCI TECH LIB

1 (PDF) CCDC ARL FCDD RLW PG E BROWN